SIGMA-1 RECEPTORS CONTROL NEUROPATHIC PAIN AND MACROPHAGE INFILTRATION INTO THE DORSAL ROOT GANGLION AFTER PERIPHERAL NERVE INJURY

Inmaculada Bravo-Caparrós[*,†,§,1], María C. Ruiz-Cantero[*,†,§,1], Gloria Perazzoli[§,#,1], , Shane J.F. Cronin[**], José M. Vela[‡], Mohamed F. Hamed[¥], Josef M. Penninger[,‡], José M. Baeyens[*,†,§], Enrique J. Cobos[*,†,§,§§,2], and Francisco R. Nieto[*,†,§,3]**

[*]Department of Pharmacology, School of Medicine, University of Granada, Granada, Spain.
[†]Institute of Neuroscience, Biomedical Research Center, University of Granada, Granada, Spain.
[§]Instituto de Investigación Biosanitaria IBS. GRANADA, Granada, Spain.
[#]Department of Human Anatomy and Embryology, School of Medicine, University of Granada, Granada, Spain.
[**]Institute of Molecular Biotechnology, Vienna, Austria.
[‡]Drug Discovery and Preclinical Development, Esteve, Barcelona, Spain.
[¥]Pathology Department, Faculty of Veterinary Medicine, Mansoura University, Mansoura, Egypt
[‡]Department of Medical Genetics, Life Science Institute, University of British Columbia, Vancouver, Canada
[§§]Teófilo Hernando Institute for Drug Discovery, Madrid, Spain.

[1]These authors contributed equally to this work.
[2]Correspondence: Department of Pharmacology, School of Medicine, University of Granada, 18016 Granada, Spain. E-mail addresses: ejcobos@ugr.es
[3]Correspondence: Department of Pharmacology, School of Medicine, University of Granada, 18016 Granada, Spain. E-mail addresses: fnieto@ugr.es

Preprint version. Please cite original version:

Bravo-Caparrós I, Ruiz-Cantero MC, Perazzoli G, Cronin SJF, Vela JM, Hamed MF, Penninger JM, Baeyens JM, Cobos EJ, Nieto FR. Sigma-1 receptors control neuropathic pain and macrophage infiltration into the dorsal root ganglion after peripheral nerve injury. FASEB J. 2020 Apr;34(4):5951-5966. https://doi.org/10.1096/fj.201901921R

ABBREVIATIONS

ATF3: activating transcription factor 3
CCL2: C-C motif chemokine ligand 2
DRG: dorsal root ganglia
FACs: fluorescence-activated cell sorting
FMO: fluorescence minus one
IBA-1: ionized calcium-binding adapter molecule 1
NeuN: neuronal nuclei
RT: room temperature
SNI: spared nerve injury
Sig-1R: sigma-1 receptor
Sig-1R-KO: sig-1R knockout
WT: wild-type

ABSTRACT
Neuron–immune interaction in the dorsal root ganglia (DRG) plays a pivotal role in neuropathic pain development after nerve injury. Sigma-1 receptor (Sig-1R) is expressed by DRG neurons but its role in neuropathic pain is not fully understood. We investigated the effect of peripheral Sig-1R on neuroinflammation in the DRG after spared (sciatic) nerve injury (SNI) in mice. Nerve injury induced a decrease in NeuN staining along with nuclear eccentricity and ATF3 expression in the injured DRG. Sig-1R was present in all DRG neurons examined, and after SNI this receptor translocated to the periphery of the soma and the vicinity of the nucleus, especially in injured ATF3+ neurons. In WT mice, injured DRG produced the chemokine CCL2, and this was followed by massive infiltration of macrophages/monocytes, which clustered mainly around sensory neurons with translocated Sig-1R, accompanied by robust IL-6 increase and mechanical allodynia. In contrast, Sig-1R knockout (Sig-1R-KO) mice showed reduced levels of CCL2, decreased macrophage/monocyte infiltration into DRG, and less IL-6 and neuropathic mechanical allodynia after SNI. Our findings point to an important role of peripheral Sig-1R in sensory neuron–macrophage/monocyte communication in the DRG after peripheral nerve injury; thus, these receptors may contribute to the neuropathic pain phenotype.

KEYWORDS: spared nerve injury; neuroinflammation; ATF3; CCL2; IL-6

INTRODUCTION

Neuropathic pain, caused by a lesion or disease of the somatosensory nervous system, has an estimated prevalence of 7–10% in the general population (1). The quality of life of patients with neuropathic pain is greatly impaired, and unfortunately, neuropathic pain management constitutes a substantially unmet clinical need (2). Therefore, understanding the pathophysiological mechanisms involved in neuropathic pain is essential to identify novel therapeutic targets and develop new analgesic drugs (3, 4).

Sigma-1 receptor (Sig-1R) is a ligand-operated chaperone with an important neuromodulatory role (5, 6). This receptor is located within the nervous system in anatomical areas important for pain control (6), where it plays a pivotal role in neuropathic pain (6, 7). Neuropathic pain-like behaviors are diminished in Sig-1R knockout (Sig-1R-KO) mice (8-11) and in wild-type (WT) animals treated with Sig-1R antagonists (9, 11, 12-15). The important effects of Sig-1R on neuropathic pain in preclinical studies have led to the development of a Sig-1R antagonist (13), which is currently under clinical development for the treatment of neuropathic pain (16, 17).

The mechanisms involved in neuropathic pain amelioration induced by Sig-1R inhibition have been studied mainly in the central nervous system, where this receptor is known to modulate central sensitization after peripheral nerve injury (reviewed in 6). Furthermore, Sig-1R inhibition decreased neuroinflammation in the spinal cord in models of pathological pain, reducing the proinflammatory cytokine content (18-20) and attenuating astrocyte and microglia activation (18, 21, 22) – changes which are all known to contribute to pain hypersensitivity (23).

In addition to central changes, chronic pain such as that produced after peripheral nerve injury also produces alterations in axotomized neurons of the dorsal root ganglia (DRG) (24-26). For example, whereas the nuclei of intact peripheral sensory neurons are located in a central position, axotomized neurons have eccentric nuclei (27), and express several transcription factors including activating transcription factor 3 (ATF3) (28). Injured DRG neurons recruit immune cells into the ganglia, mainly through the release of the chemokine CCL2 (C-C motif chemokine ligand 2) (29). The recruitment of immune cells such as peripheral macrophages into the DRG plays an active role in neuropathic pain through the local release of proinflammatory algogenic mediators which can sensitize neighboring uninjured neurons (23). Spared nerve injury (SNI) model of neuropathic pain is ideal for the study of these key features of neuropathic pain in the DRG, since the transection of the tibial and common peroneal branches of the sciatic nerve in the SNI leads to neuropathic hypersensitivity in the intact sural territory, due (at least partially) to the previously commented neuroinflammation in the affected DRG, where the somas of injured and uninjured neurons coexist (28, 30).

Interestingly, Sig-1R expression is much higher in the DRG than in the dorsal spinal cord (31), and in fact, Sig-1R is expressed by every single DRG neuron (32). We have recently described that Sig-1R inhibition attenuates neuropathic pain-like behaviors associated with the spared nerve injury (SNI) in mice (11). However, whether Sigma-1R are able to modulate neuroinflammation in the DRG is unknown.

In light of these antecedents and the gaps in our understanding of how Sig-1R influences neuropathic pain, the main aim of this study was to evaluate the possible contribution of peripheral Sig-1R to the neuroinflammation that takes place in the DRG after SNI.

MATERIAL AND METHODS

Animals

Experiments were performed in female WT (Charles River, Barcelona, Spain) and Sig-1R-KO CD-1 mice (Esteve Pharmaceuticals, Barcelona, Spain) weighing 26–32 g (8- to 11-weeks-old). Knockout mice were generated on a CD-1 background as previously described (33), by using a traditional backcrossing breeding strategy with WT progenitors from Charles River for at least 15 generations, which theoretically ensured that the genetic material from the original background is virtually absent (34). Mice harboring the mutation were then bred to homozygosity and used in this study. The animals were housed in colony cages with free access to food and water prior to the experiments. They were maintained in light- and temperature -controlled rooms (23 ± 2 °C, lights on at 07.00 h and off at 19.00 h). The animals were tested at random times throughout the estrous cycle. Animal care was in accordance with institutional (Research Ethics Committee of the University of Granada, Spain), regional (Junta de Andalucía, Spain) and international standards (European Communities Council Directive 2010/63). To decrease the number of animals in this study, we used the same mice for behavioral and in vitro studies, when possible.

Spared nerve injury

The spared nerve injury (SNI) was induced as previously described (35). Briefly, an incision was made in the left skin at the site of trifurcation of the sciatic nerve, and its three terminal branches (the sural, common peroneal and tibial nerves) were exposed. The tibial and common peroneal branches were ligated with a silk suture and transected distally, while the sural nerve was left intact. In sham-operated control mice, the sciatic nerve terminal branches were exposed but not ligated. Mice were anesthetized with isoflurane 3% (Braun VetCare, Barcelona, Spain) during the procedure. We monitor carefully for signs of distress after surgery. Although mice can move, rise and get access to food and water normally after surgery, we place some food pellets on the cage floor to facilitate access to them. Autotomy behavior was not observed in any animal following SNI during this study.

Assessment of mechanical allodynia

Mechanical thresholds were tested before surgery (baseline) and 3 and 7 days after SNI. Mechanical allodynia was assessed with von Frey filaments according to a previously described method, with slight modifications (36). On each day of evaluation the mice were habituated for 60 min in individual transparent plastic chambers (7 × 7 × 13 cm) with a floor made of wire mesh. After the adaptation period, calibrated von Frey monofilaments (Stoelting, Wood Dale, IL, USA) with bending forces that ranged from 0.02 to 2 g were applied with the up–down paradigm in the sural nerve territory, starting with the 0.6 g filament. The response to the filament was considered positive if immediate flinching, licking/biting or rapid withdrawal of the stimulated paw was observed. In each consecutive test, if there was a positive response, a weaker filament was then used; if there was no response to the filament, a stronger stimulus was then selected. Behavioral evaluations were performed by an observer blinded to the mouse genotypes in all experiments.

Assessment of burrowing behavior

Laboratory mice are fossorial animals, and therefore naturally burrow to hide from predators. This innate behavior can be used to detect distress and suffering in rodents, including neurological deficits and sickness behavior (37). More recently, burrowing behavior has been used to detect the effects of pain on the general condition of rodents (38). We used burrows whose design was adapted from (39). Burrows were made in-

house and consisted of hollow plastic tubes (68 mm diameter × 225 mm length). One end of the burrowing tube was sealed with a plastic cap. Burrows were filled with normal diet food pellets, and the open end was raised 30 mm above the cage floor, to minimize pellets drop when placed in the testing cage. Every experimental day, mice were habituated in individual cages in the testing room for 30 minutes. The first day, mice were acclimatized in their cages with the empty tube for 15 min before the burrowing assay, in order to reduce the effects of novelty. Testing was conducted during the first hour of the animals' light cycle. Burrowing behavior was tested by placing the filled tube into the cage for 30 min. The procedure was repeated three days in each animal: one training day, a second consecutive day to determine the baseline activity of burrowing before surgery and 7 days after SNI. During the period of the assay, each animal was always placed in the same cage with the same tube without food and water.
Lipopolysaccharides (LPS) administration was used as a positive control since it is known to induce sickness behavior and to dramatically reduce burrowing behavior. After determining the basal burrowing activity, LPS (L5886, Sigma-Aldrich, Madrid, Spain) at a dose of 500 µg/kg, or sterile physiological saline, was administered intraperitoneally (i.p.) in a volume of 10 ml/kg. Burrowing behavior was measured 3 hours after the injection (40).
The burrowing activity was calculated by subtracting the weight of remained pellets in the tube at the end of assay, from the starting weight of the total amount of pellets, and expressing the proportion of displaced pellets as a percentage.

Immunohistochemistry
All experiments were performed in lumbar L4 DRG, since the somas of the common peroneal/tibial branches of the sciatic nerve and those from the sural nerve in mice are located at this level (28). This made it possible to immunostain injured and non-injured neurons at this location simultaneously.

On day 7 after surgery, SNI mice were anesthetized with isoflurane 4% and perfused transcardially with 0.9% saline solution followed by 4% paraformaldehyde (Sigma-Aldrich, Madrid, Spain). The DRG were excised and post-fixed for 1 h (4 °C) in the same fixative solution. Samples were dehydrated and embedded in paraffin with standard produces. Sections of DRG were serially cut on a sliding microtome at 5 µm and mounted on microscope slides (Sigma-Aldrich). Slides containing every tenth section of L4 DRG were deparaffinized in xylol (Panreac Quimica, Castellar del Vàlles, Spain), and rehydrated with alcohol (Panreac Quimica) and distilled water before the antigen retrieval procedure (steam heating for 22 min with 1% citrate buffer, pH 8). Tissue sections were incubated for 60 min in a blocking solution that contained 5% normal goat or horse serum (Sigma-Aldrich) depending on the experiment, 0.3% Triton X-100 (Sigma-Aldrich) and 0.1% Tween 20 (Sigma-Aldrich) in Tris buffer solution at room temperature (RT). Then the slides were incubated with the primary antibodies in blocking solution. The primary antibodies used were rabbit anti-ATF3 (1:200, sc-188, Santa Cruz Biotechnology, Inc., Heidelberg, Germany), mouse anti-Sig-1R (1:200, sc-137075, Santa Cruz Biotechnology), rabbit anti-ionized calcium-binding adapter molecule 1 (IBA-1, 1:200, 019-19741, Wako Chemical, Neuss, Germany), rabbit anti-NeuN (neuronal nuclei) (1:500, ABN78, Merck Millipore, MA, USA) and rabbit anti-PGP 9.5 (1:400, AB1761, Merck Millipore). Incubation with the primary antibodies for Sig-1R, NeuN, PGP 9.5 and IBA-1 lasted for 1 h (RT), whereas incubation with the primary antibody for ATF3 lasted overnight (4 °C). After incubation with the primary antibodies, the tissue sections were washed three times for 10 min and incubated for 1 h (RT) with the appropriate secondary antibody solution containing goat anti-mouse

Alexa Fluor 488 (A11029), goat anti-rabbit Alexa Fluor 488 (A11008), or goat anti-rabbit Alexa Fluor 594 (A11012) (all 1:500, all from Life Technologies, Carlsbad, CA, USA), depending on the experiment. We also stained some tissue sections with NeuN conjugated with Alexa Fluor 555 (1:500, MAB377A5, Merck Millipore) and Alexa Fluor 488 (1:500, MAB377X, Merck Millipore).

The slides were then washed three times for 10 min and coverslipped with ProLong® Gold Antifade mounting medium (Molecular Probes; Oregon, USA). In some experiments, slides were incubated for 5 min (RT) with Hoescht 33342 (1:1000, Sigma-Aldrich) and washed three times before the mounting procedure. Slides were visualized under a confocal laser-scanning microscope (Model A1, Nikon Instruments Europe BV, Amsterdam, Netherlands) and processed with Image-J software (version 1.48, Wayne Rasband, NIH, Bethesda, MD, USA). For quantifications based on inmunohistochemical images, the data were obtained in 3–6 ipsilateral or contralateral sections per mouse, from at least 4 mice. To study macrophage infiltration into the DRG, double positive immunoreactivity for IBA-1 (as a macrophage/monocyte marker) and Hoechst 33342 was quantified in 4 areas (100 × 100 μm) located randomly in each DRG section. For the remaining quantifications, whole DRG sections were used instead of random areas. To estimate the percentage of DRG neurons with macrophage ring-like structures closely adhered to the neuronal surface, only neurons with at least 25% of their plasma membrane surrounded by IBA-1 staining were counted, as previously described (41). Quantitative data were recorded by an observer blinded to the mouse genotype and the type of sample (naive, ipsilateral or contralateral to the SNI).

Fluorescence-activated cell sorting (FACs)

For these experiments, we selected L3 and L4 DRG since they contained all somas from the common peroneal and tibial branches of the sciatic nerve (28), and therefore contained all neurons injured after SNI. Each assay was performed in samples with L3 and L4 DRG from 3 animals. The DRG were dissected and digested with collagenase IV (1 mg/mL, LS004188, Worthington, Lakewood, NJ, USA) and DNAse I (0.1%, LS002007, Worthington) for 1 h at 37 °C with agitation, and then with trypsin (0.25%, 15400054, Thermo Fisher Scientific, Massachusetts, USA) for 7 min at 37 °C with agitation. The digestion was neutralized with fetal bovine serum (FBS) (10%, 16000-036, Thermo Fisher Scientific) in phosphate-buffered saline (PBS). Cells were gently pipetted up and down to obtain a single cell suspension. Samples were filtered (pore size 35 μm) and the rat anti-CD32/16 antibody (1:100, 20 min, 553141; Biolegend, San Diego, CA) was used to block Fc-γRII (CD32) and Fc-γRIII (CD16) binding to IgG. Cells were incubated with antibodies recognizing the hematopoietic cell marker CD45 (1:200, 103108, clone 30-F11, Biolegend), the myeloid marker CD11b (1:100, 101227, clone M1/70, Biolegend), and the neutrophil-specific marker Ly6G (1:100, 127617, clone 1A8, Biolegend), together with a viability dye (1:1000, 65-0865-14, Thermo Fisher Scientific), for 30 min on ice. The populations of macrophages/monocytes (CD45+CD11b+Ly6G− cells) and neutrophils (CD45+CD11b+Ly6G+ cells) were determined from the markers indicated above in cells labelled with the viability dye.

Before and after incubation with the antibodies, the cells were washed three times in 2% FBS/PBS (FACS buffer). Cells were fixed with paraformaldehyde (2%, 158127, Sigma-Aldrich) for 20 min, and on the next day samples were assayed with a BD FACSCanto II flow cytometer (BD Biosciences, San Jose, CA, USA). Compensation beads were used as compensation controls, and fluorescence minus one (FMO) controls were included to determine the level of nonspecific staining and

autofluorescence associated with different cell subsets. All data were analyzed with FlowJo 2.0 software (Treestar, Ashland, OR, USA).

Cytokine and chemokine measurement assays in DRG

L3 and L4 DRG were excised and homogenized by sonication in 50 μL RIPA (0278, Sigma-Aldrich) supplemented with protease inhibitors (0.5%, P8340, Sigma-Aldrich) and phosphatase inhibitors (1%, P0044, Sigma-Aldrich). Ipsilateral or contralateral DRG from three mice were pooled, homogenized and tested as a single sample. Protein concentration in tissue homogenates was measured with the Bradford assay. The samples were stored at −80 °C until use.

For the determination of CCL2, twenty micrograms of protein was loaded in each well, and CCL2 levels were quantified with an enzyme-linked immunosorbent assay (ELISA) according to the manufacturer's instructions (MJE00, R&D Systems, Abingdon, United Kingdom). For the determination of IL-6, IL-1β and TNF, twenty micrograms of protein was loaded in each well, and levels of the three cytokines were quantified in the same samples with a Luminex-based multiplex immunoassay according to the manufacturer's instructions (MHSTCMAG-70K, Merck, Darmstadt, Germany)

Data analysis

For behavioral studies, statistical analyses were done with two-way repeated measures analysis of variance (ANOVA). For immunofluorescence quantification assays, statistical analyses were done with one- or two-way ANOVA, or the unpaired Student's *t* test depending on the experiment. For FACs, ELISA and multiplex studies, statistical analyses were done with two-way ANOVA. The Bonferroni post hoc test was used for all ANOVA results. The differences between values were considered significant when the *P* value was less than 0.05. All data were analyzed with SigmaPlot 12.0 software (Systat Sofware Inc, San Jose, CA, USA).

RESULTS

Sig-1R-KO mice show reduced mechanical allodynia after SNI

We compared the response to mechanical stimulation after SNI in WT and Sig-1R-KO mice. Both groups had similar von Frey thresholds in the hind paw before surgery (Fig. 1). After SNI, mechanical thresholds in the paw contralateral to surgery were similar to the baseline values in both Sig-1R-KO and WT animals (Fig. 1). No change was observed in pain thresholds in sham-operated control mice (data not shown). However, WT mice progressively developed mechanical allodynia in the injured limb, manifested as a significant reduction in the mechanical threshold in the paw ipsilateral to the injury starting 3 days after surgery, and peaking 7 days after SNI (Fig. 1). In contrast, Sig-1R-KO mice developed significantly less mechanical hypersensitivity compared to WT mice after SNI (Fig. 1).

Therefore, SNI induced sensory hypersensitivity in the injured limb but not in the side contralateral to the nerve injury in both WT and Sig-1R-KO mice. However, animals lacking Sig-1R developed attenuated neuropathic allodynia.

Burrowing behavior was not altered after SNI

We compared the burrowing behavior in WT and Sig-1R-KO mice before and after SNI. Uninjured mice from both genotypes showed a similar percentage of pellets displaced from the burrowing tube at baseline measurement and 7 days after baseline recording (Supplemental Fig. 1A), indicating that the mutant mice do not exhibit

neurological alterations which interfere with this complex behavior. Both WT and Sig-1R-KO mice, 7 days after SNI surgery showed also similar values of pellets displaced during burrowing, which were equivalent to the baseline recording (Supplemental Fig. 1A). Therefore, SNI was unable to induce any apparent decrease in burrowing behavior in either genotype. However, the percentage of pellets displaced from the burrowing tube dramatically dropped 3 hours after LPS administration to WT mice, when compared with control group administered with saline (Supplemental Fig. 1B). These results indicate that sickness behavior, in contrast to neuropathic pain, robustly interfere with this behavior.

Subcellular Sig-1R distribution in DRG is altered in injured neurons after SNI in WT mice

To study the expression of Sig-1R in the DRG after SNI, we used immunofluorescence double labeling for Sig-1R and the neuronal markers NeuN (Fig. 2A) or PGP 9.5 (Fig. 2B). The double labeling with Sig-1R and NeuN, showed that Sig-1R was expressed by all DRG neurons (NeuN-expressing cells) from naive WT mice (Fig. 2A, left panels), and that Sig-1R staining was still markedly present after SNI in DRG ipsilateral or contralateral to the surgical injury (Fig. 2A, middle and right panels). In contrast, some cells, with a clear neuronal morphology, showed Sig1-R staining in DRG ipsilateral to the SNI but no appreciable NeuN labeling (see white arrows in Fig. 2A, middle panels). Sig-1R immunolabeling was completely absent in both naive and Sig-1R-KO mice after SNI (Supplemental Fig. 2), indicating the specificity of Sig-1R staining.

At higher magnification, variable degrees of NeuN staining intensity were evident in DRG ipsilateral to the SNI. Some neurons showed faint or no staining for cytoplasmic NeuN, although they retained NeuN labeling in the nucleus (Supplemental Fig. 3, middle panels) and showed strongly positive labeling for the cellular stress marker ATF3, whereas neurons with intense NeuN labeling showed no ATF3 staining (Supplemental Fig. 3, lower panels). Neurons in DRG from naive mice and in DRG contralateral to the SNI showed prominent NeuN staining but no ATF3 labeling (Supplemental Fig. 3, left and right panels). Therefore, ATF3-expressing neurons showed less NeuN staining, and were found exclusively in injured DRG.

Immunofluorescence double labeling for NeuN and PGP 9.5 shows that whereas PGP 9.5 staining was still normally present after SNI, NeuN expression was reduced or absent in some DRG neurons (PGP 9.5+ cells) ipsilateral to the injury (Supplemental Fig. 4). These results indicate that PGP 9.5, in contrast to NeuN, stained consistently both injured and uninjured neurons. We then analyzed the double staining of Sig-1R and PGP 9.5, and confirmed that Sig-1R labeling was present in all neurons (PGP 9.5-expressing cells) either from non-injured or injured DRG samples (Fig. 2B). Higher magnification images of the double staining of Sig-1R and PGP 9.5 showed that Sig-1R labeling is restricted to PGP 9.5-expressing cells, in DRG samples from either naive or SNI mice (Fig. 3A), indicating that Sig-1R is selectively expressed in neurons in the DRG and that nerve injury does not alter this selectivity in the expression of Sig-1R.

Interestingly, most Sig-1R staining was relatively homogeneous within DRG neurons from naive mice and in DRG contralateral to the injury (Fig. 3A and 3B, left and right panels), although in some neurons Sig-1R staining was concentrated at the periphery of the soma and the vicinity of the nucleus (which was devoid of Sig-1R staining) in DRG ipsilateral to the SNI (Fig. 3A and B, middle panels). We observed markedly more Sig-1R translocation in DRG neurons from the side ipsilateral to the SNI compared to DRG from naive animals and from the side contralateral to the injury (Fig. 3C). Most of the DRG neurons with evidence of Sig-1R translocation after SNI

also had eccentric nuclei (Fig. 3A and B, middle panels). Since eccentric nuclei is a sign of axotomy, we performed double labeling of Sig-1R with ATF3. We found that most neurons showing Sig-1R translocation (78.4%) in the DRG ipsilateral to the SNI also expressed ATF3 in the cell nucleus (Fig. 3B, middle panels and Fig. 3D).

In summary, SNI induced nuclear eccentricity, a decrease in NeuN staining, and ATF3 expression in neurons from injured DRG. These changes were accompanied by a change in the subcellular distribution of Sig-1R in sensory neurons, i.e. translocation to the periphery of the soma and the vicinity of the cell nucleus.

Macrophage/monocyte infiltration and IL-6 levels in the DRG after SNI are modulated by Sig-1R

Because the infiltration of immune cells into the DRG after peripheral nerve injury plays a key role in the development of neuropathic pain (see Introduction for references), we investigated the infiltration of neutrophils and macrophages/monocytes by FACS, in DRG from WT and Sig-1R-KO mice after SNI. We did not find a significant infiltration of neutrophils (CD45+CD11b+Ly6G+ cells) in the injured DRG at day 1 or 7 after SNI in mice from either genotype (Fig. 4A). However, we found a markedly greater presence of macrophages/monocytes (CD45+CD11b+Ly6G− cells) in injured DRG from WT mice on day 7 after SNI compared to naive DRG, and this increase was largely attenuated in Sig-1R-KO mice (Fig. 4A). DRG samples from the side contralateral to the injury from either WT or Sig-1R-KO mice did not show any significant increase in the number of either neutrophils or macrophages/monocytes (Fig. 4B).

Next, we further investigate by immunohistochemistry the macrophage/monocyte infiltration into DRG from WT and Sig-1R-KO mice after SNI. Figure 5 shows representative images for the neuronal marker NeuN and the macrophage/monocyte marker IBA-1 in DRG from non-injured WT and Sig-1R-KO mice, and from samples obtained 7 days after SNI in both genotypes (Fig. 5A). In naive WT and Sig-1R-KO animals, little or no appreciable IBA-1 staining was detected (Fig. 5A, left panels). However, after SNI, macrophages/monocytes clustered around the cell bodies of neurons producing ring-like structures in DRG ipsilateral to the injury in WT mice, and these neurons often showed decreased NeuN labeling (white arrows in Fig. 5A, middle panels). IBA1+ cells were still present in Sig-1R-KO animals, but at much lower levels than in WT mice (Fig.5A, middle panels). The quantification of IBA-1+ cells confirmed the considerable infiltration of macrophages/monocytes into ipsilateral DRG in WT mice after SNI (compared to samples from naive animals and samples from the side contralateral to the injury), and also showed that the increase in macrophage/monocyte numbers in the DRG was smaller in Sig-1R-KO animals (Fig. 5B). These results are evidence that SNI induced massive macrophage/monocyte infiltration into the DRG, and that infiltration was markedly weaker in mice that lacked Sig-1R. Accordingly, these findings suggest that Sig-1R plays an important role in macrophage/monocyte recruitment after nerve injury.

We then measured by a multiplex immunoassay the levels of proinflammatory cytokines related to macrophages/monocytes (IL-6, IL-1β and TNF) in DRG from injured and non-injured WT and Sig-1R-KO mice, at day 7 after SNI. The concentrations of IL-1β and TNF were below the detection limit of the assay that we employed (data not shown). Non-injured WT and Sig-1R-KO mice had similar levels of IL-6 (Fig. 5C). In contrast, the concentration of IL-6 in injured DRG from both WT and Sig-1R-KO mice was significantly increased, although at a much lower extent in Sig-1R-KO mice than in WT mice (Fig. 5C). Therefore, the lower infiltration of

macrophages/monocytes into injured DRG in Sig-1R-KO mice that we described above, was accompanied by a reduction in the levels of IL-6.

We next further investigated the relationship between macrophages/monocytes infiltration and the Sig-1R in the DRG following SNI. For this purpose, we carried out immunofluorescence double labeling with Sig-1R and the macrophage/monocyte marker IBA-1 in WT mice. Figure 6A shows representative images for Sig-1R and IBA-1 staining in DRG from naive animals, injured animals, and samples from the side contralateral to the injury. In naive animals little or no appreciable IBA-1 staining was detected (Fig. 6A, left panels). However, after SNI, macrophages/monocytes clustered around the cell bodies in Sig-1R-stained neurons, forming the previously commented ring-like structures in the DRG ipsilateral to the injury (Fig. 6A, middle panels). However, few or no IBA-1+ cells were detected in DRG contralateral to the nerve injury (Fig. 6A, right panels). We observed a minimal overlapping between Sig-1R and IBA-1 labeling in the regions where the neuron and macrophage/monocyte are closest (Fig. 6A, middle panels), supporting the close neuron–immune cell interaction, and suggesting that Sig-1R was expressed in sensory neurons but not in macrophages or monocytes. The characteristic ring-like IBA-1 labeling was seen mostly in neurons with Sig-1R staining at the periphery of the soma (Fig. 6A middle panels). In fact, a majority (69.5%) of neurons with Sig-1R translocation to the periphery of the soma were surrounded by macrophages/monocytes, whereas these immune cells rarely accumulated around neurons that did not show evidence of Sig-1R translocation: only 20.5% of neurons without translocation were surrounded by IBA-1+ cells (Fig. 6B). These results suggested that Sig-1R might be involved in the communication between neurons and macrophages/monocytes.

Sig-1R-KO mice show lower levels of CCL2 in the DRG after SNI than WT mice

To investigate whether Sig-1R might be relevant for macrophage/monocyte recruitment, we next measured the levels of the chemokine CCL2 in DRG from non-injured WT and Sig-1R-KO mice, as well as at several time-points after SNI in samples from both genotypes. Non-injured mice from both the WT and Sig-1R-KO groups had similar baseline levels of CCL2. The concentration of CCL2 in injured DRG from WT mice showed a bell-shaped time-course, increasing as early as 24 h after surgery, peaking on day 3 after the injury, and subsequently decreasing on day 7 (Fig. 7). Sig-1R-KO mice also had increased levels of CCL2 in DRG ipsilateral to the SNI, with a time-course similar to that in WT mice, but the increase in CCL2 content was significantly smaller that in WT mice (Fig. 7). The increase in CCL2 was restricted to injured DRG, given that CCL2 concentration did not change at any time-point tested in the DRG contralateral to the injury in either WT or Sig-1R-KO mice. These results suggest that Sig-1R modulated CCL2 release in the DRG after SNI.

DISCUSSION

We show that Sig-1R-KO mice develop less mechanical allodynia than WT mice in response to peripheral nerve injury. Spared nerve injury was followed by the presence of eccentric nuclei, a decrease in NeuN staining, and ATF3 expression in neurons from injured DRG. These changes were accompanied by Sig-1R translocation to the plasma membrane (or nearby areas) and the vicinity of the cell nucleus in peripheral sensory neurons. In addition, we found an increase in the levels of CCL2, macrophage/monocyte numbers and IL-6, in injured DRG. These immune cells formed ring-like structures mainly in neurons in which Sig-1R was translocated. In Sig-1R-KO

mice the levels of CCL2, macrophage/monocyte infiltration and IL-6 into the DRG were lower after nerve injury than in WT mice.

Peripheral nerve injuries such as nerve transection that takes place during surgical procedures or as a consequence of other trauma lead to neuropathic pain in a considerable number of patients (42, 43). Here we show that mechanical allodynia in the intact sural branch territory of mice, after transection of the common peroneal and tibial branches of the sciatic nerve (i.e. SNI), developed progressively in WT animals, with a time-course similar to that reported in previous studies based on mouse models (11, 30, 44). We show that Sig-1R-KO mice developed significantly less mechanical allodynia than WT mice after SNI. This result is in agreement with our recent study in the same neuropathic pain model (11), and with previous reports that mutant animals lacking Sig-1R developed less sensory hypersensitivity than WT mice in other neuropathic pain models (8-10, 45).

We also found that uninjured WT and Sig-1R-KO mice showed a similar burrowing behavior. Although Sig-1R have a known pivotal role on neurotransmission (46, 47), this might be more prominent in pain pathways than in other systems, as its absence in the mutant mice does not lead to an overt behavioral dysfunction. We show that SNI did not depressed burrowing behavior in either WT or Sig-1R-KO mice. Although it has been reported that neuropathic pain in rodents decrease burrowing or other innate behaviors such as exploratory activity (e.g. 48, 49), this is not always the case (50). LPS-induced sickness behavior inhibited burrowing activity, as previously reported (40), suggesting that the lack of effect of SNI on this behavior is not due to methodological issues. Therefore, although SNI induces prominent allodynia, it does not impact on the functionality of the rodents in our burrowing experimental conditions.

We found that Sig-1R immunoreactivity in normal conditions was expressed in the somas of all peripheral sensory neurons from the mouse DRG. The receptor was located in the cytoplasm but not inside the cell nucleus, as previously reported (32, 51). We show that Sig-1R staining in sensory neurons changed dramatically after nerve injury only in DRG from the side ipsilateral to SNI, where it accumulated in the plasma membrane (or nearby areas) and in close proximity to the cell nucleus. We demonstrated the specificity of the antibody used for Sig-1R staining by verifying the absence of immunoreactivity in samples from Sig-1R-KO mice before and after SNI. It was previously reported that when Sig-1R is activated by either sigma-1 agonism or cellular stress, it translocates from its intracellular location to the plasmalemmal area within the extended endoplasmic reticulum (or to the plasma membrane itself) and to the nuclear envelope (52, 53, 54). Therefore, the alterations we observed in Sig-1R labeling induced by SNI might indicate that nerve injury triggered Sig-1R activation. To our knowledge, this is the first experimental evidence that changes in the subcellular distribution of Sig-1R are identifiable in DRG neurons after nerve injury. Further studies using specific subcellular markers are guaranteed to deepen on the study of this process in sensory neurons.

We show that some DRG neurons from the side ipsilateral to SNI underwent other changes in addition to the alterations in subcellular Sig-1R distribution, including nuclear eccentricity, which has long been known to be due to severe neuronal damage (27, 55), and a marked decrease in NeuN staining. To our knowledge there are no previously published studies in DRG tissues that document the decrease in NeuN labeling after nerve injury. However, recent studies have questioned the reliability of NeuN immunoreactivity as a marker for neuron numbers during certain pathological states (56, 57). In particular, it is known that NeuN staining decreases markedly after axotomy in several nervous system structures, whereas other neuronal markers do not

(e.g. 56, 57). In fact, in the present study, we found that the expression of PGP 9.5 (another neuronal marker) did not change in DRG neurons ipsilateral to the injury, in contrast to the marked decrease in NeuN staining. This decrease in NeuN staining we observed in the DRG may reflect changes in injured neurons since it was accompanied by a clear increase in ATF3 labeling in the neuronal nucleus – a finding of relevance given that ATF3 is considered among the most reliable markers of injury in DRG neurons (28, 58). Importantly, we observed that the majority of DRG neurons with Sig-1R translocation also expressed ATF3, suggesting that Sig-R1 activation (translocation) was mostly restricted to injured neurons.

It is known that nerve injury induces immune cell infiltration into the affected DRG (59). We found a marked increase in macrophages/monocytes in the DRG after peripheral nerve injury, in agreement with previous studies (30, 60). We did not observe increased neutrophil recruitment in the DRG after nerve injury, which is also in agreement with previous reports (61). We show that macrophages/monocytes accumulated and formed ring-like structures mostly in sensory neurons where Sig-1R was translocated. It was previously reported that these ring-like structures are seen preferentially in injured neurons (41), a finding consistent with the Sig-1R translocation we report here in injured neurons. The accumulation of macrophages/monocytes around neurons with translocated Sig-1R may indicate that Sig-1R activation is important for the interaction between these immune cells and injured sensory neurons. In support of this hypothesis, we show here that in Sig-1R-KO mice, macrophage/monocyte infiltration into the DRG after nerve injury was much weaker than in WT mice. It is worth noting that under our experimental conditions, labeling for the Sig-1R in DRG samples was restricted to sensory neurons, either before or after nerve injury. Therefore, the modulation by Sig-1R of macrophage/monocyte infiltration in the DRG after nerve injury is unlikely to be attributable to direct sigma-1-mediated effects on these immune cells or other cell types, but rather can be explained by curtailed communication between neurons and macrophages/monocytes.

The communication between peripheral sensory neurons and immune cells is complex, but currently the role of CCL2 in this interaction is unquestioned. This chemokine has potent chemotactic activity and is involved in macrophage recruitment in the DRG after nerve injury (62). In this connection, it is well known that injured neurons are the main source of this chemokine in DRG after nerve injury (e.g. 29, 63, 64). In fact, CCL2 blockade results in a decrease in the number of macrophages/monocytes that migrate into the DRG after nerve injury (e.g. 61, 65). Thus CCL2 is one of the main molecules that mediate macrophage/monocyte recruitment by injured neurons in the DRG. Here we show that CCL2 was produced soon after nerve injury, with a bell-shaped time-course. The levels of CCL2 increased as early as 1 day after injury, reached a maximum at 3 days, but subsequently decreased 7 days after the injury. This time-course of CCL2 production after peripheral nerve injury is consistent with at least one previous report in another mouse model (63). According to the present findings, Sig-1R-KO mice had reduced levels of this chemokine in the injured DRG after SNI, and this lower activity may partly account for the decreased macrophage/monocyte infiltration in the DRG in our mutant animals after nerve injury.

Macrophage and monocyte recruitment into the DRG plays a pivotal role in neuropathic pain, because they promote a proinflammatory environment in the affected ganglia which can in turn sensitize non-injured neurons, and thus contribute to the development of sensory hypersensitivity in the intact sural branch territory after SNI (30, 66). We found a significant increase in the levels of the proinflammatory cytokine IL-6 in the injured DRG following SNI, in agreement with previous studies (41, 67),

which was attenuated in Sig-1R-KO mice. Since proinflammatory macrophages are the primary source of IL-6 after nerve injury (60, 62), the reduced levels of IL-6 in injured DRG of Sig-1R-KO mice might be explained by the reduced infiltration of macrophages/monocytes found at this location. In addition, both CCL2 and IL-6 have direct effects on sensory neurons in that they increase their excitability (68, 69, 70), and importantly, gene expression of both proinflammatory mediators in DRG of human patients has been recently reported to be associated to neuropathic pain (71). Altogether, the decrease in CCL2 levels and the reduced macrophage/monocyte infiltration into the DRG after nerve injury in Sig-1R-KO mice, with the consequent decrease in IL-6, may contribute to the lower sensory hypersensitivity we observed in these mutant animals. Our results are summarized in Fig. 8.

It was previously reported that Sig-1R antagonism is also able to decrease microglia recruitment and astrocyte activation in the dorsal horn during pathological pain conditions, and this might contribute to the known ameliorative effects of Sig-1R inhibition on sensory hypersensitivity (18, 21, 22). It is interesting to note that CCL2 released from primary afferents into the spinal cord also participates in microglia recruitment and astrocyte activation in the spinal dorsal horn (29, 72). Therefore, in light of the present results, it can be hypothesized that at least part of the previously described central effects induced by Sig-1R inhibition during pain conditions may be attributable to the actions of this receptor on peripheral sensory neurons, rather than to its direct central effects. The development of peripherally-restricted Sig-1R ligands or the knockout of Sig-1R in specific subsets of DRG neurons would aid for the study of the peripheral actions of these receptors.

In summary, we found that nerve injury triggered the activation of Sig-1R in peripheral sensory neurons, and that this receptor played a key role in the recruitment of macrophages/monocytes into the injured DRG, and were thus directly involved in a process that is crucial for the development of neuropathic pain. Therefore, Sig-1R inhibition may be a potentially effective approach to alleviating neuropathic pain not only because of its previously described central effects, but also because of its clear, simultaneous actions at the peripheral level.

ACKNOWLEDGEMENTS

I. Bravo-Caparrós and M. C. Ruiz-Cantero were supported by FPU grants from the Spanish Ministry of Education, Culture and Sports. This study was partially supported by the Spanish Ministry of Economy and Competitiveness (MINECO, grant SAF2016-80540-R), the Junta de Andalucía (grant CTS 109), and funding from Esteve Pharmaceuticals and the European Regional Development Fund (ERDF). This research was done in partial fulfillment of the requirements for the doctoral degree awarded to I. Bravo-Caparrós. The authors thank Mohamed Tassi Mzanzi and Ana Santos Carro for their technical support with confocal microscopic image acquisition, Gustavo Ortíz Ferrón for his technical support in the FACs experiments, and Daniel Pérez Bartivas for his assistance with microphotograph analysis. The authors acknowledge K. Shashok for improving the use of English in the manuscript. The authors declare no conflicts of interest.

AUTHOR CONTRIBUTIONS

J. M. Baeyens, E. J. Cobos and F. R. Nieto, designed research; I. Bravo-Caparrós, G. Perazzoli, M. C. Ruiz-Cantero, M. F. Hamed and F. R. Nieto, performed research; I. Bravo-Caparrós, JM Vela, F. R. Nieto, S. J. Cronin, J. M. Penninger, E. J. Cobos and J. M. Baeyens, analyzed data; I. Bravo-Caparrós, M. C. Ruiz-Cantero, J. M. Baeyens, E. J. Cobos and F. R. Nieto, wrote the paper. All authors read and approved the final version of the manuscript.

REFERENCES

1. Colloca, L., Ludman, T., Bouhassira, D., Baron, R., Dickenson, A.H., Yarnitsky, D., Freeman, R., Truini, A., Attal, N., Finnerup, N.B., Eccleston, C., Kalso, E., Bennett, D. L., Dworkin, R.H., and Raja, S.N. (2017) Neuropathic pain. *Nat. Rev. Dis. Primers* **3**, 17002
2. Finnerup, N.B., Attal, N., Haroutounian, S., McNicol, E., Baron, R., Dworkin, R.H., Gilron, I., Haanpää, M., Hansson, P., Jensen, T.S., Kamerman, P.R., Lund, K., Moore, A., Raja, S.N., Rice, A.S., Rowbotham, M., Sena, E., Siddall, P., Smith, B.H., and Wallace, M. (2015) Pharmacotherapy for neuropathic pain in adults: a systematic review and meta-analysis. *Lancet Neurol.* **14**, 162-173
3. Jay, G.W., and Barkin, R.L. (2014) Neuropathic pain: etiology, pathophysiology, mechanisms, and evaluations. *Dis. Mon.* **60**, 6-47
4. St John Smith, E. (2018) Advances in understanding nociception and neuropathic pain. *J. Neurol.* **265**, 231-238
5. Su, T.P., Su, T.C., Nakamura, Y., and Tsai, S.Y. (2016) The sigma-1 receptor as a pluripotent modulator in living systems. *Trends Pharmacol. Sci.* **37**, 262-278
6. Sánchez-Fernández, C., Entrena, J.M., Baeyens, J.M., and Cobos, E.J. (2017) Sigma-1 receptor antagonists: a new class of neuromodulatory analgesics. *Adv. Exp. Med. Biol.* **964**, 109-132.
7. Merlos, M., Romero, L., Zamanillo, D., Plata-Salamán, C., and Vela, J.M. (2017) Sigma-1 receptor and pain. *Handb. Exp. Pharmacol.* **244**, 131-161
8. de la Puente, B., Nadal, X., Portillo-Salido, E., Sánchez-Arroyos, R., Ovalle, S., Palacios, G., Muro, A., Romero, L., Entrena, J.M., Baeyens, J.M., López-García, J.A., Maldonado, R., Zamanillo, D., and Vela, J.M. (2009) Sigma-1 receptors regulate activity-induced spinal sensitization and neuropathic pain after peripheral nerve injury. *Pain* **145**, 294-303
9. Nieto, F.R., Cendán, C.M., Sánchez-Fernández, C., Cobos, E.J., Entrena, J.M., Tejada, M.A., Zamanillo, D., Vela, J.M., and Baeyens, J.M. (2012) Role of sigma-1 receptors in paclitaxel-induced neuropathic pain in mice. *J. Pain* **13**, 1107-1121.
10. Nieto, F.R., Cendán, C.M., Cañizares, F.J., Cubero, M.A., Vela, J.M., Fernández-Segura, E., and Baeyens, J.M. (2014) Genetic inactivation and pharmacological blockade of sigma-1 receptors prevent paclitaxel-induced sensory-nerve mitochondrial abnormalities and neuropathic pain in mice. *Mol. Pain* **10**, 11
11. Bravo-Caparrós, I., Perazzoli, G., Yeste, S., Cikes, D., Baeyens, J.M., Cobos, E.J., and Nieto, F.R. (2019) Sigma-1 receptor inhibition reduces neuropathic pain induced by partial sciatic nerve transection in mice by opioid-dependent and -independent mechanisms. *Front. Pharmacol.* **10**, 613
12. Roh, D.H., Kim, H.W., Yoon, S.Y., Seo, H.S., Kwon, Y.B., Kim, K.W., Han, H.J., Beitz, A.J., Na, H.S., and Lee, J.H. (2008) Intrathecal injection of the sigma1 receptor antagonist BD1047 blocks both mechanical allodynia and increases in spinal NR1 expression during the induction phase of rodent neuropathic pain. *Anesthesiology* **109**, 879-889
13. Romero, L., Zamanillo, D., Nadal, X., Sánchez-Arroyos, R., Rivera-Arconada, I., Dordal, A., Montero, A., Muro, A., Bura, A., Segales, C., Laloya, M., Hernández, E., Portillo-Salido, E., Escriche, M., Codony, X., Encina, G., Burgueno, J., Merlos, M., Baeyens, J.M., Giraldo, J., López-García, J.A., Maldonado, R., Plata-Salaman, C.R., and Vela, J.M. (2012) Pharmacological properties of S1RA, a new sigma-1 receptor antagonist that inhibits neuropathic pain and activity-induced spinal sensitization. *Br. J. Pharmacol.* **166,** 2289-2306

14. Gris, G., Portillo-Salido, E., Aubel, B., Darbaky, Y., Deseure, K., Vela, J. M., Merlos, M., and Zamanillo, D. (2016) The selective sigma-1 receptor antagonist E-52862 attenuates neuropathic pain of different aetiology in rats. *Sci. Rep.* **6**, 24591
15. Kang D.W., Moon, J.Y., Choi, J.G., Kang, S.Y., Ryu, Y., Park, J.B., Lee, J.H., and Kim, H.W. (2016) Antinociceptive profile of levo-tetrahydropalmatine in acute and chronic pain mice models: role of spinal sigma-1 receptor. *Sci. Rep.* **6**, 37850
16. Abadias, M., Escriche, M., Vaqué, A., Sust, M., and Encina, G. (2013) Safety, tolerability and pharmacokinetics of single and multiple doses of a novel sigma-1 receptor antagonist in three randomized phase I studies. *Br. J. Clin. Pharmacol.* **75**, 103-117
17. Bruna, J., Videla, S., Argyriou, A.A., Velasco, R., Villoria, J., Santos, C., Nadal, C., Cavaletti, G., Alberti, P., Briani, C., Kalofonos, H.P., Cortinovis, D., Sust, M., Vaqué, A., Klein, T., and Plata-Salamán, C. (2018) Efficacy of a novel sigma-1 receptor antagonist for oxaliplatin-induced neuropathy: a randomized, double-blind, placebo-controlled phase IIa clinical trial. *Neurotherapeutics* **15**, 178-189
18. Zhu, S., Wang, C., Han, Y., Song, C., Hu, X., and Liu, Y. (2015) Sigma-1 receptor antagonist BD1047 reduces mechanical allodynia in a rat model of bone cancer pain through the inhibition of spinal NR1 phosphorylation and microglia activation. *Mediators Inflamm.* **2015***,* 265056
19. Castany, S., Gris, G., Vela, J.M., Verdú, E., and Boadas-Vaello, P. (2018) Critical role of sigma-1 receptors in central neuropathic pain-related behaviours after mild spinal cord injury in mice. *Sci. Rep.*; **8**, 3873
20. Castany, S., Codony, X., Zamanillo, D., Merlos, M., Verdú, E., and Boadas-Vaello, P. (2019) Repeated sigma-1 receptor antagonist MR309 administration modulates central neuropathic pain development after spinal cord injury in mice. *Front. Pharmacol.* **10,** 222
21. Jeong, Y.C., Son, J.S., and Kwon, Y.B. (2015) The spinal antinociceptive mechanism determined by systemic administration of BD1047 in zymosan-induced hyperalgesia in rats. *Brain Res. Bull.* **119**, 93-100
22. Choi, S.R., Kwon, S.G., Choi, H.S., Han, H.J., Beitz, A.J., and Lee, J.H. (2016) Neuronal NOS activates spinal NADPH oxidase 2 contributing to central sigma-1 receptor-induced pain hypersensitivity in mice. *Biol. Pharm. Bull.* **39,** 1922-1931
23. Ji, R.R., Chamessian, A., and Zhang, Y.Q. (2016) Pain regulation by non-neuronal cells and inflammation. *Science* **354**, 572-577
24. Zimmermann, M. (2001) Pathobiology of neuropathic pain. *Eur. J. Pharmacol.* **429**, 23-37
25. Hu, G., Huang, K., Hu, Y., Du, G., Xue, Z., Zhu, X., and Fan, G. (2016) Single-cell RNA-seq reveals distinct injury responses in different types of DRG sensory neurons. *Sci. Rep.* **6**, 31851
26. Wiberg, R., Novikova, L.N., and Kingham, P.J. (2018) Evaluation of apoptotic pathways in dorsal root ganglion neurons following peripheral nerve injury. *Neuroreport* **29**, 779-785
27. Johnson, I.P., and Sears, T.A. (2013) Target-dependence of sensory neurons: An ultrastructural comparison of axotomised dorsal root ganglion neurons with allowed or denied reinnervation of peripheral targets. *Neuroscience* **228**, 163-178
28. Laedermann, C.J., Pertin, M., Suter, M.R., and Decosterd, I. (2014) Voltage-gated sodium channel expression in mouse DRG after SNI leads to re-evaluation of projections of injured fibers. *Mol. Pain* **10,** 19
29. Zhu, X., Cao, S., Zhu, M.D., Liu, J.Q., Chen, J.J., and Gao, Y.J. (2014) Contribution of chemokine CCL2/CCR2 signaling in the dorsal root ganglion and spinal

cord to the maintenance of neuropathic pain in a rat model of lumbar disc herniation. *J. Pain* **15**, 516-526
30. Cobos, E.J., Nickerson, C.A., Gao, F., Chandran, V., Bravo-Caparrós, I., González-Cano, R., Riva, P., Andrews, N.A., Latremoliere, A., Seehus, C.R., Perazzoli, G., Nieto, F.R., Joller, N., Painter, M.W., Ma, C.H.E., Omura, T., Chesler, E.J., Geschwind, D.H., Coppola, G., Rangachari, M., Woolf, C.J., and Costigan, M. (2018) Mechanistic differences in neuropathic pain modalities revealed by correlating behavior with global expression profiling. *Cell Rep.* **22**, 1301-1312
31. Sánchez-Fernández, C., Montilla-García, Á., González-Cano, R., Nieto, F.R., Romero, L., Artacho-Cordón, A., Montes, R., Fernández-Pastor, B., Merlos, M., Baeyens, J.M., Entrena, J.M., and Cobos, E.J. (2014) Modulation of peripheral μ-opioid analgesia by σ_1 receptors. *J. Pharmacol. Exp. Ther.* **348,** 32-45
32. Montilla-García, Á., Perazzoli, G., Tejada, M.Á., González-Cano, R., Sánchez-Fernández, C., Cobos, E.J., and Baeyens, J.M. (2018) Modality-specific peripheral antinociceptive effects of μ-opioid agonists on heat and mechanical stimuli: Contribution of sigma-1 receptors. *Neuropharmacology* **135**, 328-342
33. Entrena, J.M., Cobos, E.J., Nieto, F.R., Cendán, C.M., Gris, G., Del Pozo, E., Zamanillo, D., and Baeyens, J.M. (2009) Sigma-1 receptors are essential for capsaicin-induced mechanical hypersensitivity: studies with selective sigma-1 ligands and sigma-1 knockout mice. *Pain* **143**, 252-261
34. Wong, G.T. (2002) Speed congenics: applications for transgenic and knock-out mouse strains. *Neuropeptides* **36**,230-236
35. Decosterd, I., and Woolf, C.J. (2000) Spared nerve injury: an animal model of persistent peripheral neuropathic. *Pain* **87**, 149–158
36. Chaplan, S.R., Bach, F.W., Pogrel, J.W., Chung, J.M., and Yaksh, Y.T. (1994) Quantitative assessment of tactile allodynia in the rat paw. J. Neurosci. *Methods* **53**, 55–63
37. Deacon, R.M. (2006) Burrowing in rodents: a sensitive method for detecting behavioral dysfunction. *Nat. Protoc.* **1**, 118-121
38. Cobos, E.J., and Portillo-Salido, E. (2013) "Bedside-to-bench" behavioral outcomes in animal models of pain: beyond the evaluation of reflexes. *Curr. Neuropharmacol*. **11**, 560-591
39. Deacon, R. (2012) Assessing burrowing, nest construction, and hoarding in mice. *J Vis Exp*. **59**, e2607
40. Püntener, U., Booth, S.G., Perry, V.H., and Teeling, J.L. (2012) Long-term impact of systemic bacterial infection on the cerebral vasculature and microglia. *J Neuroinflammation* **9**,146
41. Vega-Avelaira, D., Géranton, S.M., and Fitzgerald, M. (2009) Differential regulation of immune responses and macrophage/neuron interactions in the dorsal root ganglion in young and adult rats following nerve injury. *Mol. Pain* **5**, 70
42. Borsook, D., , Kussman, B.D., George, E., Becerra, L.R., and Burke, D.W. (2013) Surgically induced neuropathic pain: understanding the perioperative process. *Ann. Surg.* **257**, 403-412
43. Hewson, D.W., Bedforth, N.M., and Hardman, J.G. (2018) Peripheral nerve injury arising in anaesthesia practice. *Anaesthesia* **73**, 51-60
44. Bourquin, A.F., Süveges, M., Pertin, M., Gilliard, N., Sardy, S., Davison, A.C., Spahn, D. R., and Decosterd, I. (2006) Assessment and analysis of mechanical allodynia-like behavior induced by spared nerve injury (SNI) in the mouse. *Pain* **122**, e1-14

45. Wang, X., Feng, C., Qiao, Y., and Zhao, X. (2018) Sigma 1 receptor mediated HMGB1 expression in spinal cord is involved in the development of diabetic neuropathic pain. *Neurosci. Lett.* **668**, 164-168
46. van Waarde, A., Ramakrishnan, N.K., Rybczynska, A.A., Elsinga, P.H., Ishiwata, K., Nijholt, I.M., Luiten, P.G., and Dierckx, R.A. (2011) The cholinergic system, sigma-1 receptors and cognition. *Behav Brain Res*. **221,** 543-554
47. Kourrich, S. (2017) Sigma-1 receptor and neuronal excitability. in sigma proteins: evolution of the concept of sigma receptors. (Kim, F., Pasternak, G., eds) Vol. 244, pp. 109-124, Handbook of Experimental Pharmacology, Springer, Cham
48. Urban, R., Scherrer, G., Goulding, E. H., Tecott, L. H., and Basbaum, A. I. (2011) Behavioral indices of ongoing pain are largely unchanged in male mice with tissue or nerve injury-induced mechanical hypersensitivity. *Pain* **152**, 990-1000
49. Shepherd, A. J., Cloud, M. E., Cao, Y. Q., and Mohapatra, D. P. (2018) Deficits in burrowing behaviors are associated with mouse models of neuropathic but not inflammatory pain or migraine. *Front. Behav. Neurosci.* **12**, 124
50. Sheahan, T. D., Siuda, E. R., Bruchas, M. R., Shepherd, A. J., Mohapatra, D. P., Gereau, R. W. 4th, and Golden, J. P. (2017) Inflammation and nerve injury minimally affect mouse voluntary behaviors proposed as indicators of pain. *Neurobiol. Pain* **2**, 1-12
51. Mavlyutov, T.A., Duellman, T., Kim, H.T., Epstein, M.L., Leese, C., Davletov, B.A., and Yang, J. (2016) Sigma-1 receptor expression in the dorsal root ganglion: reexamination using a highly specific antibody. *Neuroscience* **331**, 148-157
52. Su, T.P., Hayashi, T., Maurice, T., Buch, S., and Ruoho, A.E. (2010) The sigma-1 receptor chaperone as an inter-organelle signaling modulator. *Trends Pharmacol. Sci.* **31**, 557–566
53. Tsai, S.Y., Chuang, J.Y., Tsai, M.S., Wang, X.F., Xi, Z.X., Hung, J.J., Chang, W.C., Bonci, A., and Su, T.P. (2015) Sigma-1 receptor mediates cocaine-induced transcriptional regulation by recruiting chromatin-remodeling factors at the nuclear envelope. *Proc. Natl. Acad. Sci. USA* **112**, E6562-E6570
54. Liu, D. Y., Chi, T. Y., Ji, X. F., Liu, P., Qi, X. X., Zhu, L., Wang, Z. Q., Li, L., Chen, L., and Zou, L. B. (2018) Sigma-1 receptor activation alleviates blood-brain barrier dysfunction in vascular dementia mice. *Exp Neurol*. **308,** 90-99.
55. Matthews, M.R., and Raisman, G. (1972) A light and electron microscopic study of the cellular response to axonal injury in the superior cervical ganglion of the rat. *Proc. R. Soc. Lond. B. Biol. Sci.* **181**, 43-79
56. Collombet, J.M., Masqueliez, C., Four, E., Burckhart, M.F., Bernabé, D., Baubichon, D., and Lallement, G. (2006) Early reduction of NeuN antigenicity induced by soman poisoning in mice can be used to predict delayed neuronal degeneration in the hippocampus. *Neurosci. Lett.* **398**, 337-342
57. Duan, W., Zhang, Y.P., Hou, Z., Huang, C., Zhu, H., Zhang, C.Q., and Yin, Q. (2016) Novel insights into NeuN: from neuronal marker to splicing regulator. *Mol. Neurobiol.* **53**, 1637-1647
58. Tsujino, H., Kondo, E., Fukuoka, T., Dai, Y., Tokunaga, A., Miki, K., Yonenobu, K., Ochi, T., and Noguchi, K. (2000) Activating transcription factor 3 (ATF3) induction by axotomy in sensory and motoneurons: A novel neuronal marker of nerve injury. *Mol. Cell Neurosci.* **15**, 170-182
59. Scholz, J., and Woolf, C.J. (2007) The neuropathic pain triad: neurons, immune cells and glia. *Nat. Neurosci.* **10,** 1361-1368
60. Kwon, M.J., Kim, J., Shin, H., Jeong, S.R., Kang, Y.M., Choi, J.Y., Hwang, D.H., and Kim, B.G. (2013) Contribution of macrophages to enhanced regenerative

capacity of dorsal root ganglia sensory neurons by conditioning injury. *J. Neurosci.* **33**, 15095-15108
61. Lindborg, J.A., Niemi, J.P., Howarth, M.A., Liu, K. W., Moore, C.Z., Mahajan, D., and Zigmond, R.E. (2018) Molecular and cellular identification of the immune response in peripheral ganglia following nerve injury. *J. Neuroinflammation* **15,** 192
62. Zigmond, R.E., and Echevarria, F.D. (2019) Macrophage biology in the peripheral nervous system after injury. *Prog. Neurobiol.* **173**, 102-121
63. Kwon, M.J., Shin, H.Y., Cui, Y., Kim, H., Thi, A.H., Choi, J.Y., Kim, E.Y., Hwang, D. H., and Kim, B.G. (2015) CCL2 mediates neuron-macrophage interactions to drive proregenerative macrophage activation following preconditioning injury. *J. Neurosci.* **35**, 15934-15947
64. Liu, C., Luan, S., OuYang, H., Huang, Z., Wu, S., Ma, C., Wei, J., and Xin, W. (2016) Upregulation of CCL2 via ATF3/c-Jun interaction mediated the Bortezomib-induced peripheral neuropathy. *Brain Behav. Immun.* **53**, 96-104
65. Niemi, J.P., DeFrancesco-Lisowitz, A., Roldán-Hernández, L., Lindborg, J.A., Mandell, D., and Zigmond, R.E. (2013) A critical role for macrophages near axotomized neuronal cell bodies in stimulating nerve regeneration. *J. Neurosci.* **33**, 16236-16248
66. Raoof, R., Willemen, H.L.D.M., and Eijkelkamp, N. (2018) Divergent roles of immune cells and their mediators in pain. *Rheumatology (Oxford)* **57**, 429–440
67. Vallejo, R., Tilley, D. M., Williams, J., Labak, S., Aliaga, L., and Benyamin, R. M. (2013) Pulsed radiofrequency modulates pain regulatory gene expression along the nociceptive pathway. *Pain Physician.* **16**, E601-E613
68. White, F.A., Sun, J., Waters, S.M., Ma, C., Ren, D., Ripsch, M., Steflik, J., Cortright, D. N., Lamotte, R.H., and Miller, R.J. (2005) Excitatory monocyte chemoattractant protein-1 signaling is up-regulated in sensory neurons after chronic compression of the dorsal root ganglion. *Proc. Natl. Acad. Sci. USA* **102**, 14092-14097
69. Wang, C.H., Zou, L.J., Zhang, Y.L., Jiao, Y.F., and Sun, J.H. (2010) The excitatory effects of the chemokine CCL2 on DRG somata are greater after an injury of the ganglion than after an injury of the spinal or peripheral nerve. *Neurosci. Lett.* **475**, 48-52
70. Zhou, Y. Q., Liu, Z., Liu, Z. H., Chen, S. P., Li, M., Shahveranov, A., Ye, D. W., and Tian, Y. K. (2016) Interleukin-6: an emerging regulator of pathological pain. *J Neuroinflammation.* **13,** 141
71. North, R. Y., Li, Y., Ray, P., Rhines, L. D., Tatsui, C. E., Rao, G., Johansson, C. A., Zhang, H., Kim, Y. H., Zhang, B., Dussor, G., Kim, T. H., Price, T. J., and Dougherty, P. M. (2019) Electrophysiological and transcriptomic correlates of neuropathic pain in human dorsal root ganglion neurons. *Brain* **142,** 1215-1226
72. Van Steenwinckel, J., Reaux-Le Goazigo, A., Pommier, B., Mauborgne, A., Dansereau, M.A., Kitabgi, P., Sarret, P., Pohl, M., and Mélik Parsadaniantz, S. (2011) CCL2 released from neuronal synaptic vesicles in the spinal cord is a major mediator of local inflammation and pain after peripheral nerve injury. *J. Neurosci.* **31**, 5865-5875

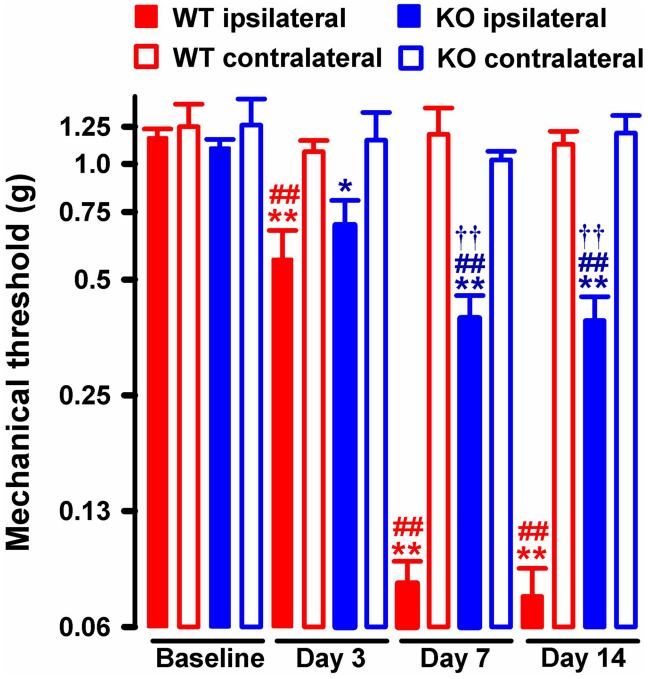

Figure 1. Comparison of spared nerve injury-induced (SNI) neuropathic mechanical allodynia in wild-type and Sig-1R-knockout mice. Von Frey thresholds were recorded 1 day before (baseline) and 3 and 7 days after SNI in the paws ipsilateral and contralateral to the site of surgery. Each bar and vertical line represent the mean ± SEM of the values obtained in 8–12 animals. Statistically significant differences between the values obtained in the same paw on the day before surgery (baseline) and different days after SNI: ** $P < 0.01$, * $P < 0.05$; between ipsilateral and contralateral measurements: ## $P < 0.01$; and between wild-type (WT) and sigma-1 knockout (KO) groups stimulated the in paw ipsilateral to SNI: †† $P < 0.01$ (two-way repeated measures ANOVA followed by Bonferroni test).

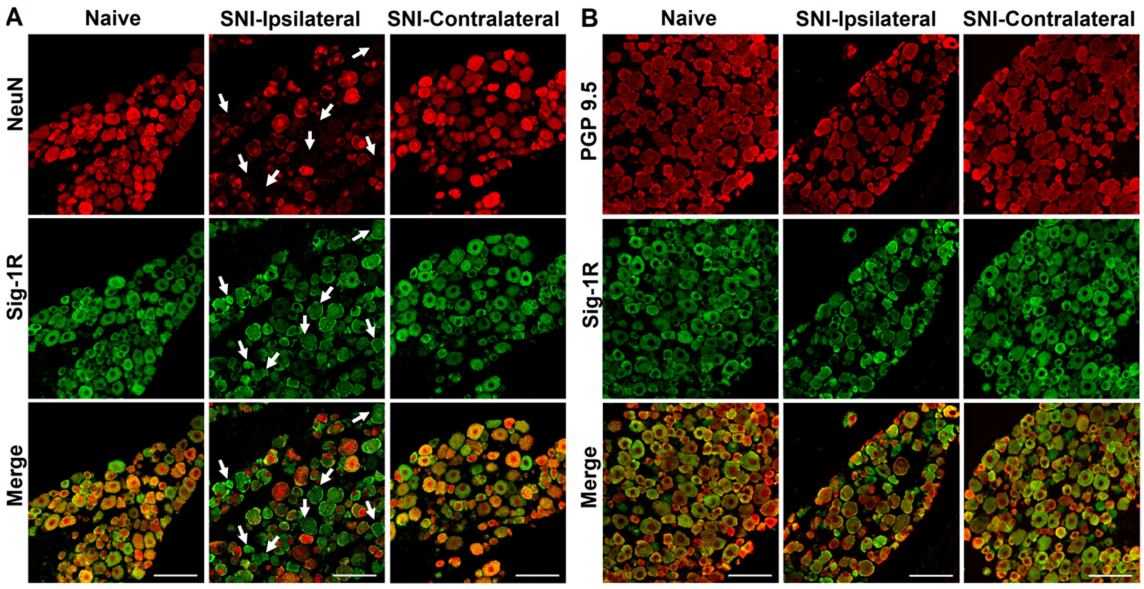

Figure 2. Double staining of sigma-1 receptor with the neuronal markers NeuN and PGP9.5 in the DRG from naive and spared nerve injury (SNI) wild-type mice. (A) Sigma-1 receptor staining (Sig-1R, green) in the DRG persists after SNI in wild-type mice, whereas NeuN labeling (red) decreases ipsilateral to SNI. Arrows indicate neurons with decreased NeuN staining and clear Sig-1R labeling. (B) Sig-1R labeling (green) is present in all PGP 9.5-expressing cells (red) either from non-injured or injured DRG samples. Images show representative microphotographs from double immunostainings in L4 DRG from naive mice, and ipsilateral and contralateral L4 DRG from mice with SNI 7 days after surgery. Scale bar 100 µm.

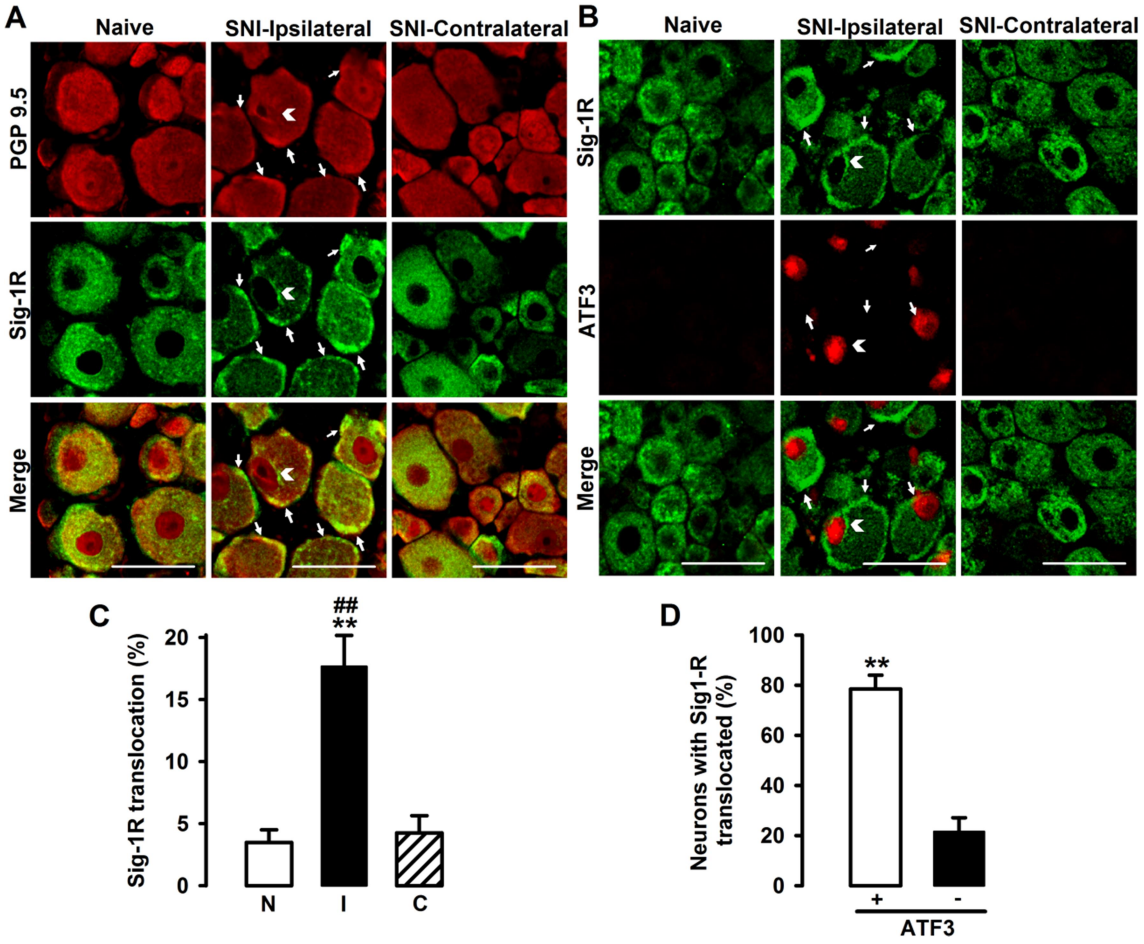

Figure 3. The subcellular distribution of sigma-1 receptor is altered in injured neurons in DRG from wild-type mice after spared nerve injury (SNI). (A) and (B) Representative microphotographs from double immunostaining for sigma-1 receptor (Sig-1R, green), PGP 9.5 (red, A) and ATF3 (red, B) in L4 DRG from naive mice, and ipsilateral and contralateral L4 DRG from mice with SNI 7 days after surgery. Arrows indicate neurons with Sig-1R staining concentrated at the periphery of the soma. Arrowheads indicate neurons with Sig-1R concentrated in close vicinity to the cell nucleus. Scale bar 50 µm. (C) Quantification of neurons showing Sig-1R translocation in samples from naive animals, and in DRG ipsilateral and contralateral to SNI. N: naive, I: ipsilateral; C: contralateral. Statistically significant differences between naive and ipsilateral groups: $^{**}P < 0.01$; and between the values in the ipsilateral and contralateral groups: $^{\#\#} P < 0.01$ (one-way ANOVA followed by Bonferroni test). (D) Quantification of the percentage of neurons with Sig-1R translocation that did or did not express ATF3. Statistically significant differences between the values in ATF3+ and ATF3− neurons with translocated Sig-1R: $^{**}P < 0.01$ (Student's *t* test). Each bar and vertical line represent the mean ± SEM of the values obtained in 4 animals in both graphs.

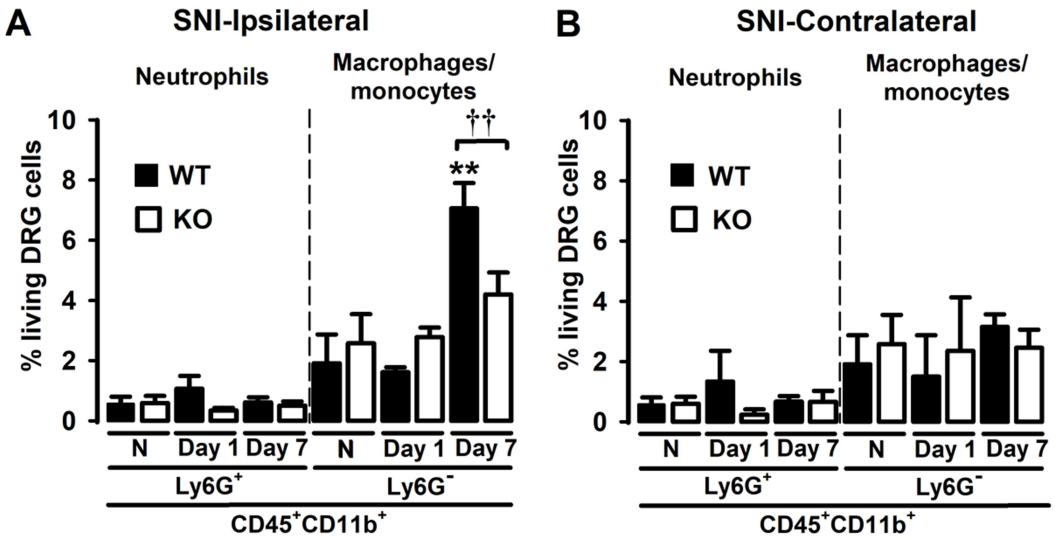

Figure 4. Spared nerve injury (SNI) induces macrophage/monocyte infiltration in the DRG of wild-type mice, which is reduced in sigma-1 receptor knockout mice, whereas there is no apparent neutrophil infiltration in DRG from either genotype. Macrophage/monocyte (CD45+CD11b+Ly6G− cells) and neutrophils (CD45+CD11b+Ly6G+ cells) were determined by FACS in DRG from naive mice, and ipsilateral (A) and contralateral (B) DRG from mice with SNI, 1 and 7 days after surgery. Each bar and vertical line represent the mean ± SEM of the values obtained in 4 or 5 batches of DRG. Each batch was obtained with L3 and L4 DRG from 3 animals. Statistically significant differences between the values in naive and SNI ipsilateral groups: ** $P < 0.01$; and between DRG ipsilateral to SNI in the WT and KO groups: †† $P < 0.01$ (two-way ANOVA followed by Bonferroni test).

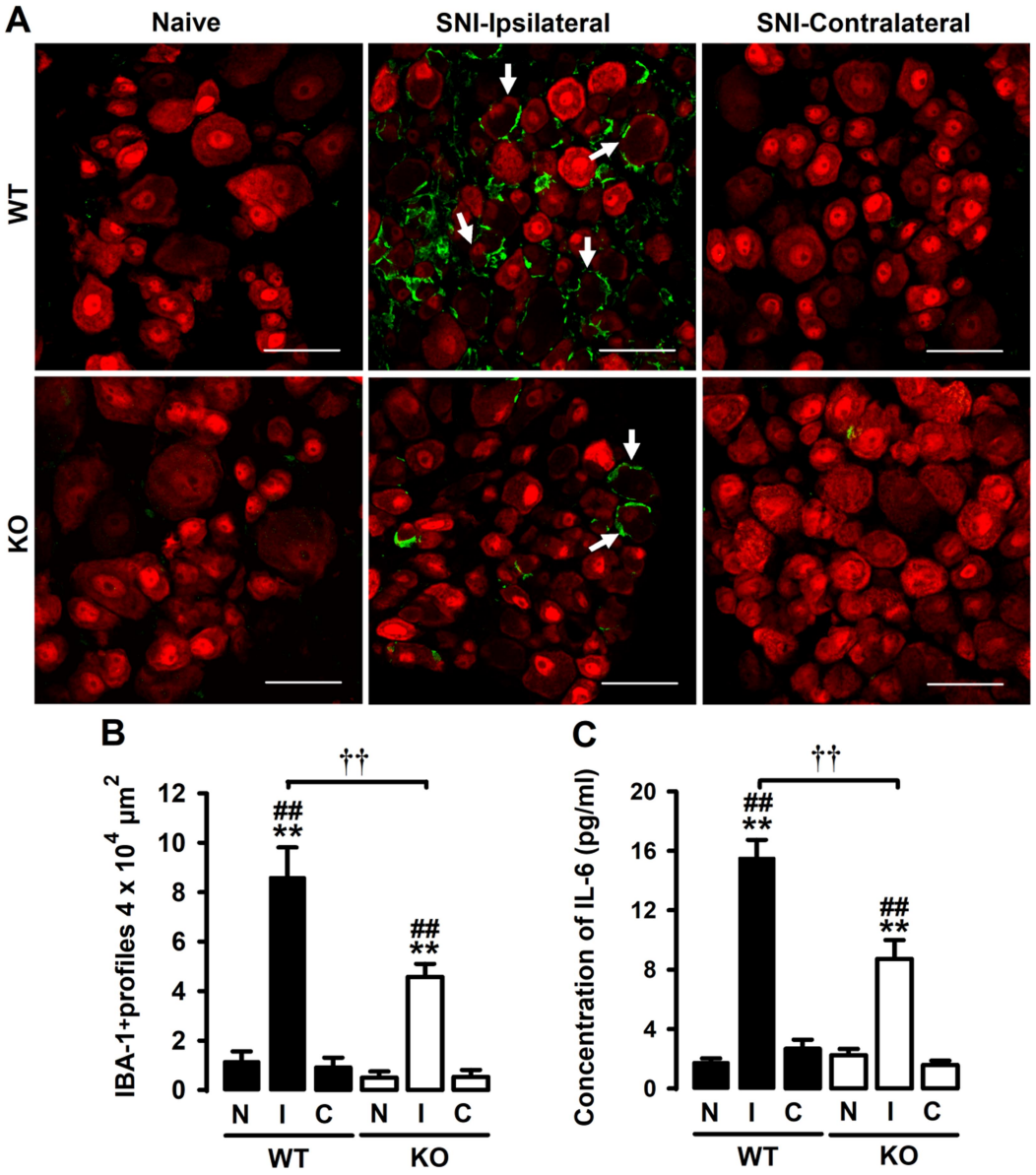

Figure 5. Sigma-1 receptor knockout mice show less macrophage/monocyte infiltration and reduced levels of IL-6 in comparison to wild-type mice in the DRG after spared nerve injury (SNI). (A) Representative microphotographs of double immunostaining for IBA-1 (green) and NeuN (red) in L4 DRG from naive mice, and ipsilateral and contralateral L4 DRG from mice with SNI 7 days after surgery. Experiments were performed in wild-type (WT) mice and sigma-1 knockout mice (KO). Scale bar 50 µm. (B) Quantification of the number of macrophages/monocytes (IBA1+ profiles) per 4 × 10^4 µm^2. Each bar and vertical line represent the mean ± SEM of the values obtained in 3–6 animals. N: naive, I: ipsilateral, C: contralateral. (C) IL-6 levels in L3 and L4 DRG ipsilateral and contralateral to SNI in wild-type (WT) and sigma-1 receptor knockout (KO) mice measured by a multiplex immunoassay. Each point and vertical line represents the mean ± SEM of the values obtained in 3–5 batches of DRG samples. Each batch was obtained with L3 and L4 DRG from 3 animals. (B and C) Statistically significant differences between the values in naive and SNI ipsilateral groups: ** $P < 0.01$; between ipsilateral and contralateral groups of mice with the same genotype: ## $P < 0.01$; and between DRG ipsilateral to SNI in the WT and KO groups: †† $P < 0.01$ (two-way ANOVA followed by Bonferroni test).

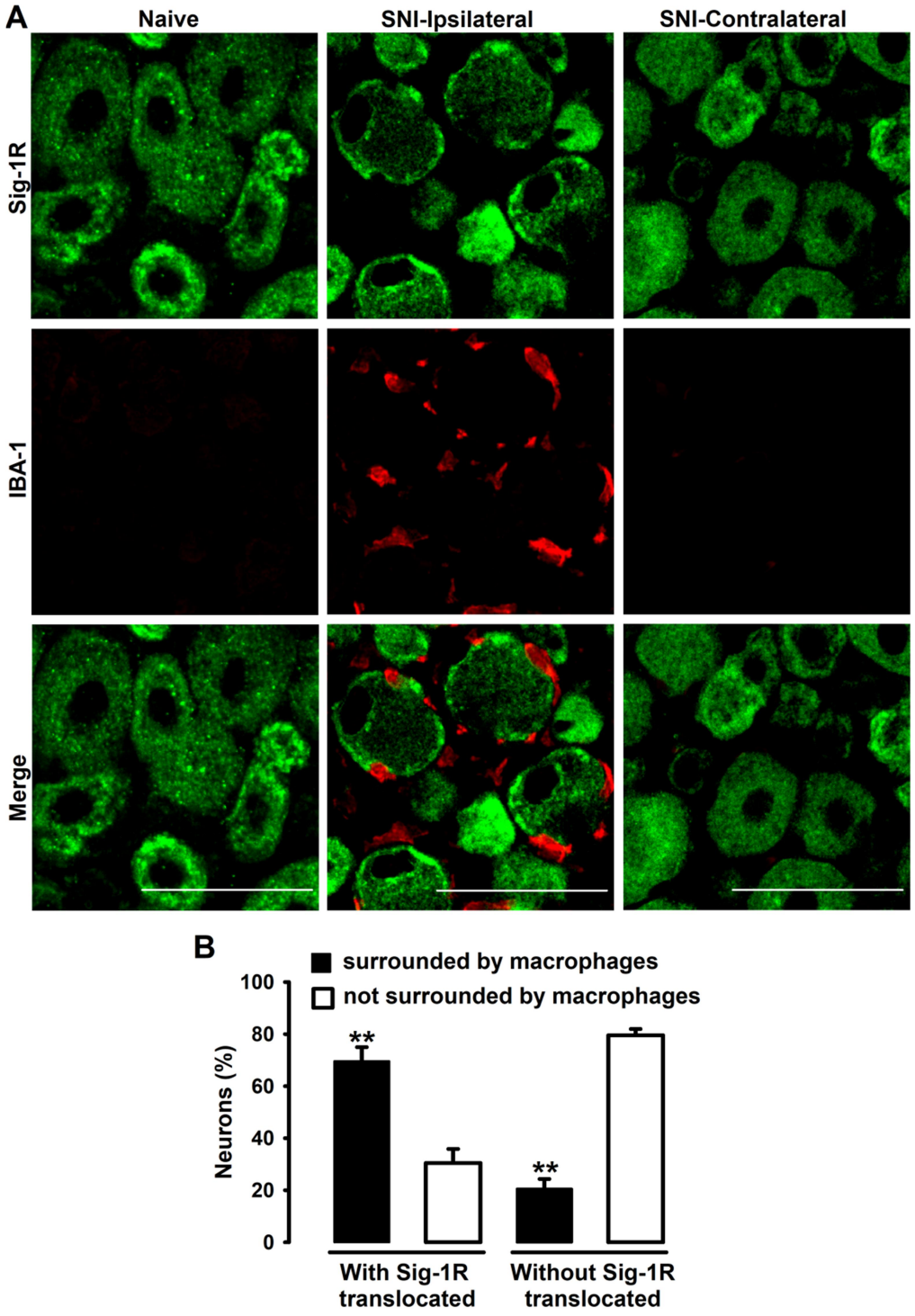

Figure 6. DRG neurons with sigma-1 receptor translocation are surrounded by macrophages/monocytes forming ring-like structures after spared nerve injury (SNI). (A) Representative microphotographs from double immunostaining for sigma-1 receptor (Sig-1R, green) and IBA-1 (red) in L4 DRG from naive mice, and ipsilateral and contralateral L4 DRG from mice with SNI 7 days after surgery. Scale bar 50 µm. (B) Quantification of the percentage of neurons with and without Sig-R1 translocation, and surrounded by macrophages or not. Each bar and vertical line represent the mean ± SEM of the values obtained in 4 animals. Statistically significant differences between the values in the groups surrounded and not surrounded by macrophages: ** $P < 0.01$ (two-way ANOVA followed by Bonferroni test).

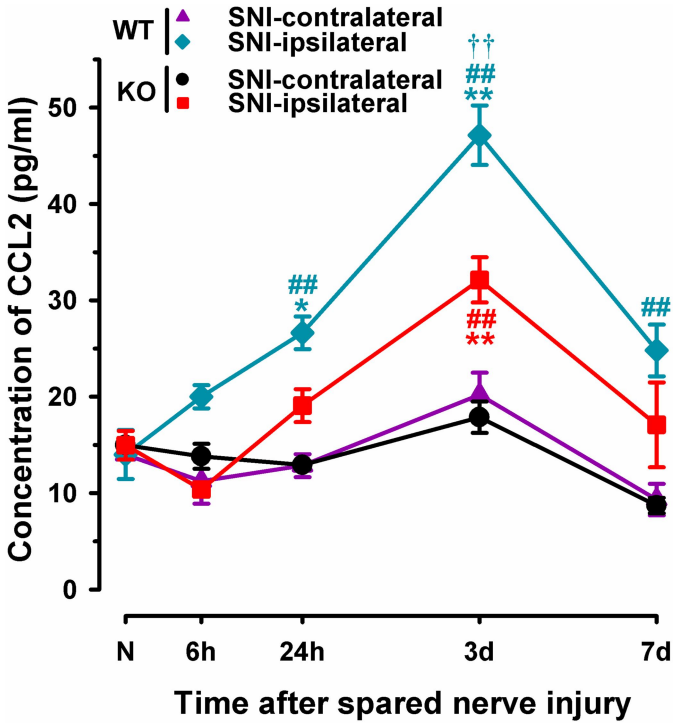

Figure 7. Sigma-1 receptor knockout mice show lower CCL2 levels in DRG after spared nerve injury (SNI) than wild-type mice. CCL2 levels in L3 and L4 DRG ipsilateral and contralateral to SNI in wild-type (WT) and sigma-1 receptor knockout (KO) mice were measured by ELISA. Each point and vertical line represents the mean ± SEM of the values obtained in 3–5 batches of DRG samples for each time point. Each batch was obtained with L3 and L4 DRG from 3 animals. Statistically significant differences between the values from DRG samples from naive and SNI mice: * $P < 0.05$, ** $P < 0.01$; between the values in DRG samples ipsilateral and contralateral to SNI within the same genotype: ## $P < 0.01$; and between the values in DRG ipsilateral to SNI in the WT and KO groups: †† $P < 0.01$ (two-way ANOVA followed by Bonferroni test).

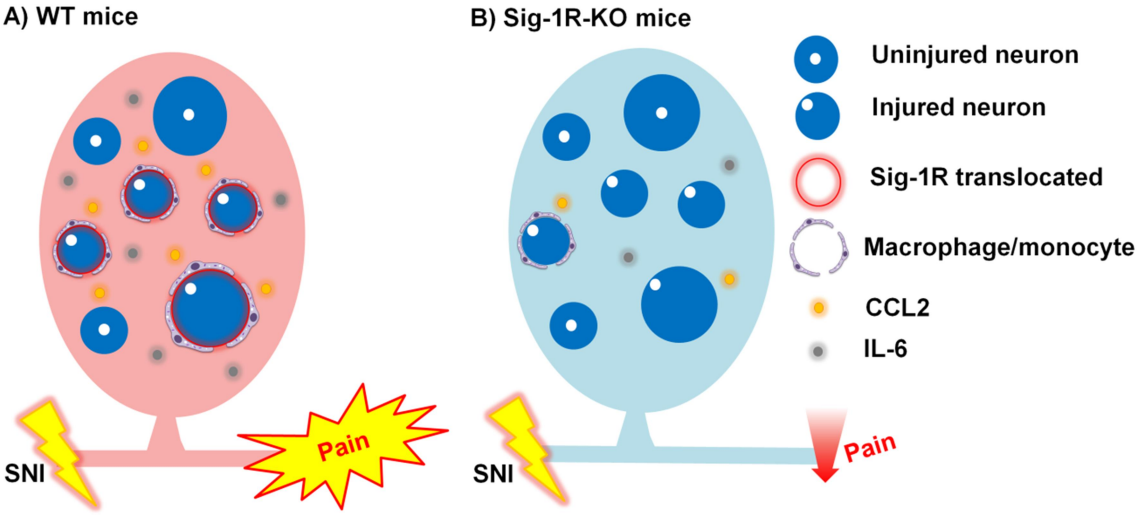

Figure 8. Proposed actions for the effects of sigma-1 receptor on DRG neuroinflammation after nerve injury. In wild-type (WT) mice, injured DRG exhibits high levels of CCL2 and a massive infiltration of macrophages/monocytes, which clustered mainly around sensory neurons with translocated sigma-1 receptor (Sig-1R), accompanied by robust IL-6 increase and mechanical allodynia as a feature of neuropathic pain. In contrast, Sig-1R knockout (Sig-1R-KO) mice showed reduced levels of CCL2, decreased macrophage/monocyte infiltration into DRG, and less IL6 and neuropathic mechanical allodynia after SNI.

SUPPLEMENTARY FIGURES

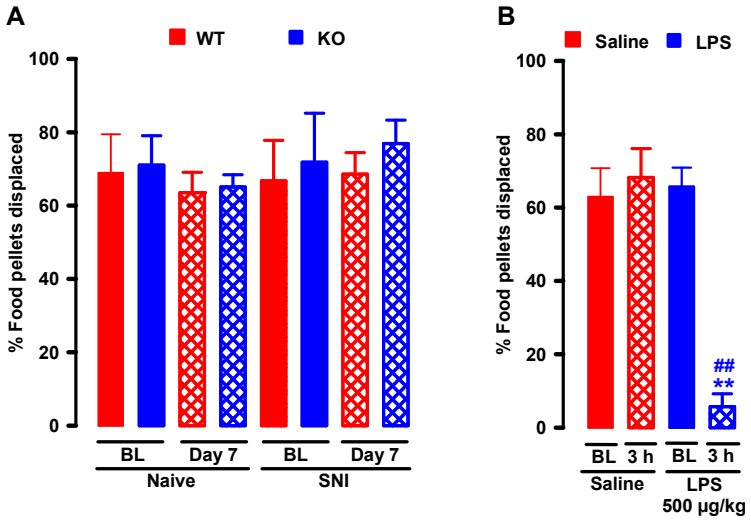

Suppl. Fig. 1. LPS administration but not spared nerve injury (SNI) induces alterations in burrowing behavior. (A) Weight of food pellets burrowed in 30 minutes by wild-type (WT) and Sig-1R-knockout mice (KO) mice submitted or not to SNI, is similar regardless of the genotype and injury. (B) LPS, administered 3h before testing, reduces significantly burrowing behavior in comparison with the saline-injected control group. Each bar and vertical line represent the mean ± SEM of the values obtained in 7–11 animals. Statistically significant differences between the values obtained before the treatment with LPS (baseline) and 3 hours after: ** $P < 0.01$; and between saline or LPS treatments: ## $P < 0.01$ (Two-way repeated measures ANOVA followed by Bonferroni test).

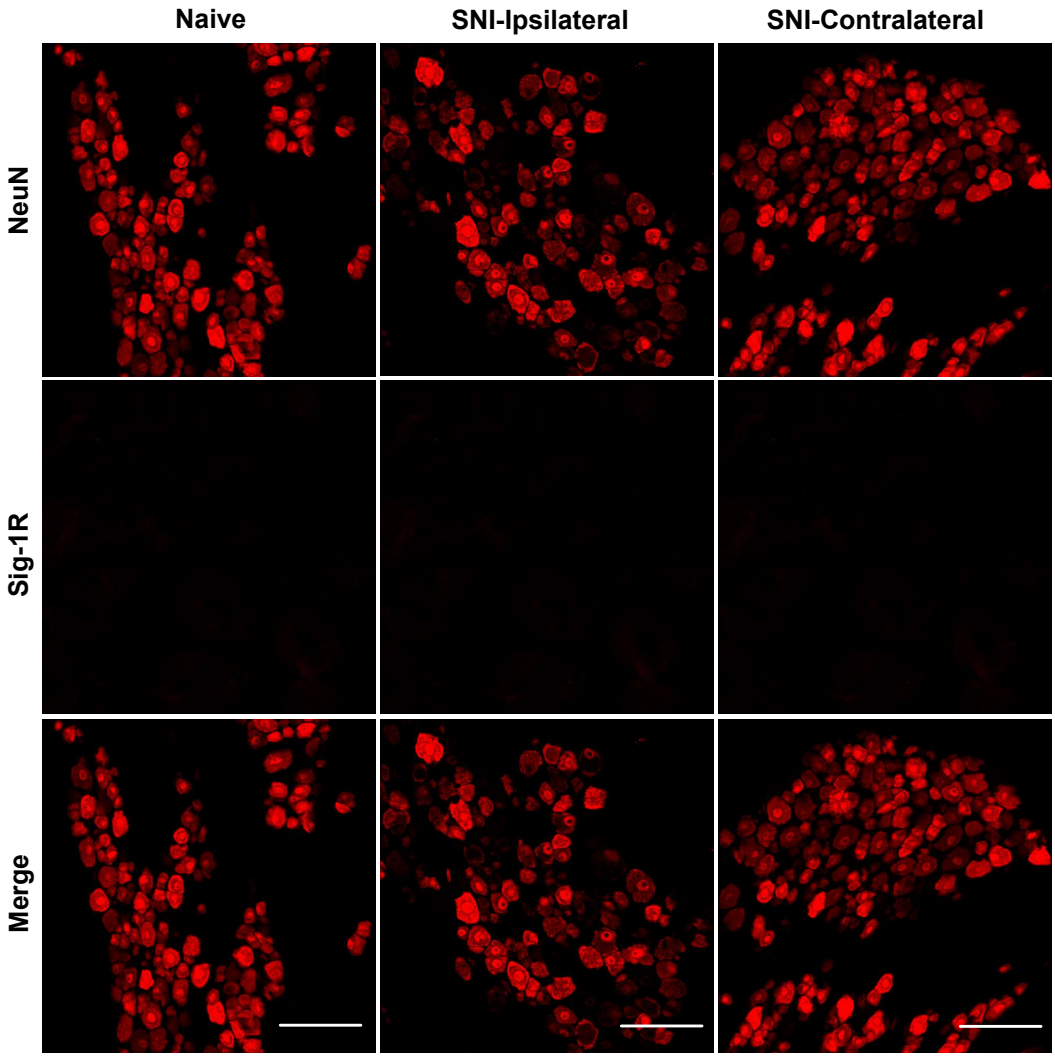

Suppl. Fig. 2. DRG samples from sigma-1 receptor knockout mice are devoid of sigma-1 receptor inmunostaining. Representative microphotographs from double immunostaining for NeuN (red) and sigma-1 receptor (Sig-1R, green) in L4 DRG from Sig-1R knockout naive mice, and ipsilateral and contralateral L4 DRG from mutant mice with spared nerve injury (SNI) 7 days after surgery. Scale bar 100 μm

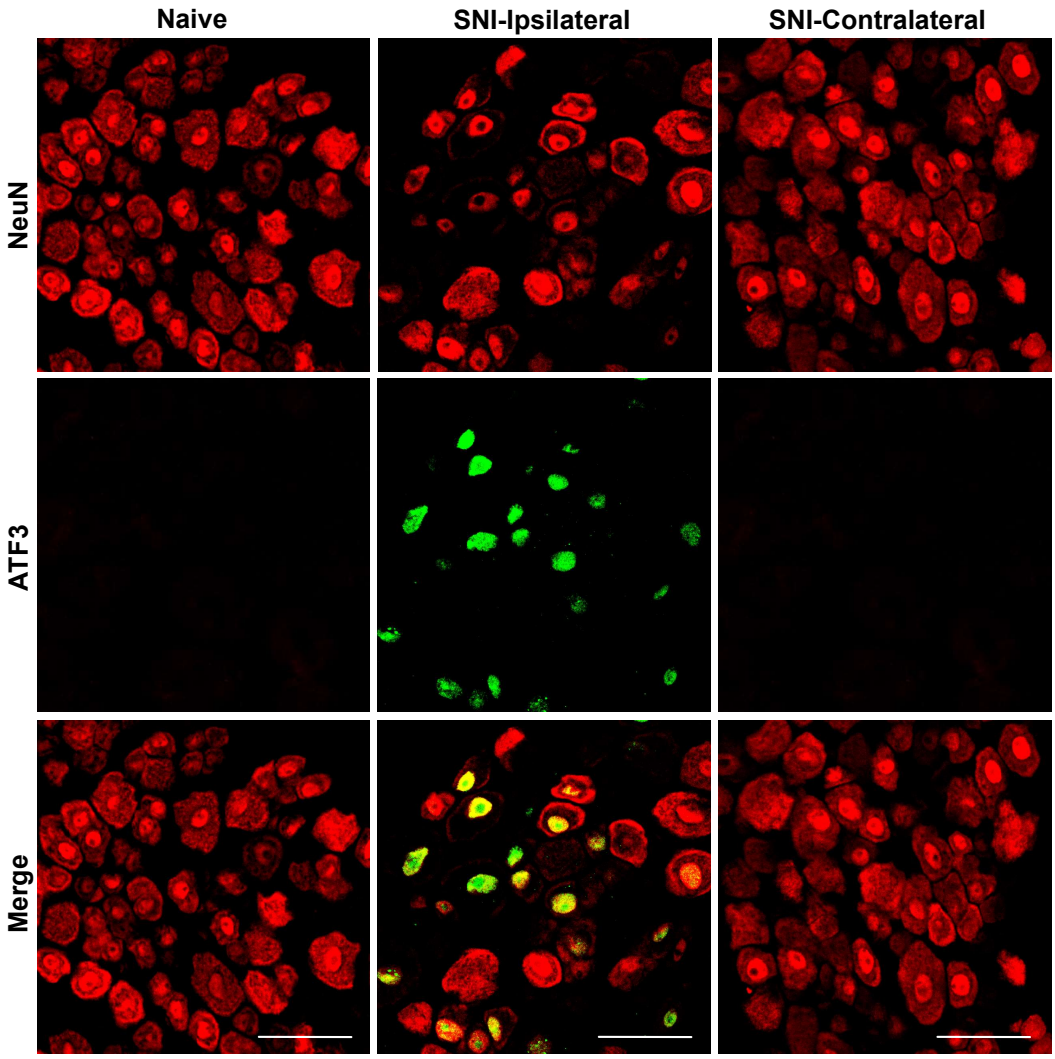

Suppl. Fig. 3. DRG neurons express ATF3 in wild-type mice after spared nerve injury (SNI), and show decreased NeuN staining. Representative microphotographs from double immunostaining for NeuN (red) and ATF3 (green) in L4 DRG from naive mice, and ipsilateral and contralateral L4 DRG from mice with SNI 7 days after surgery. Scale bar 50 μm.

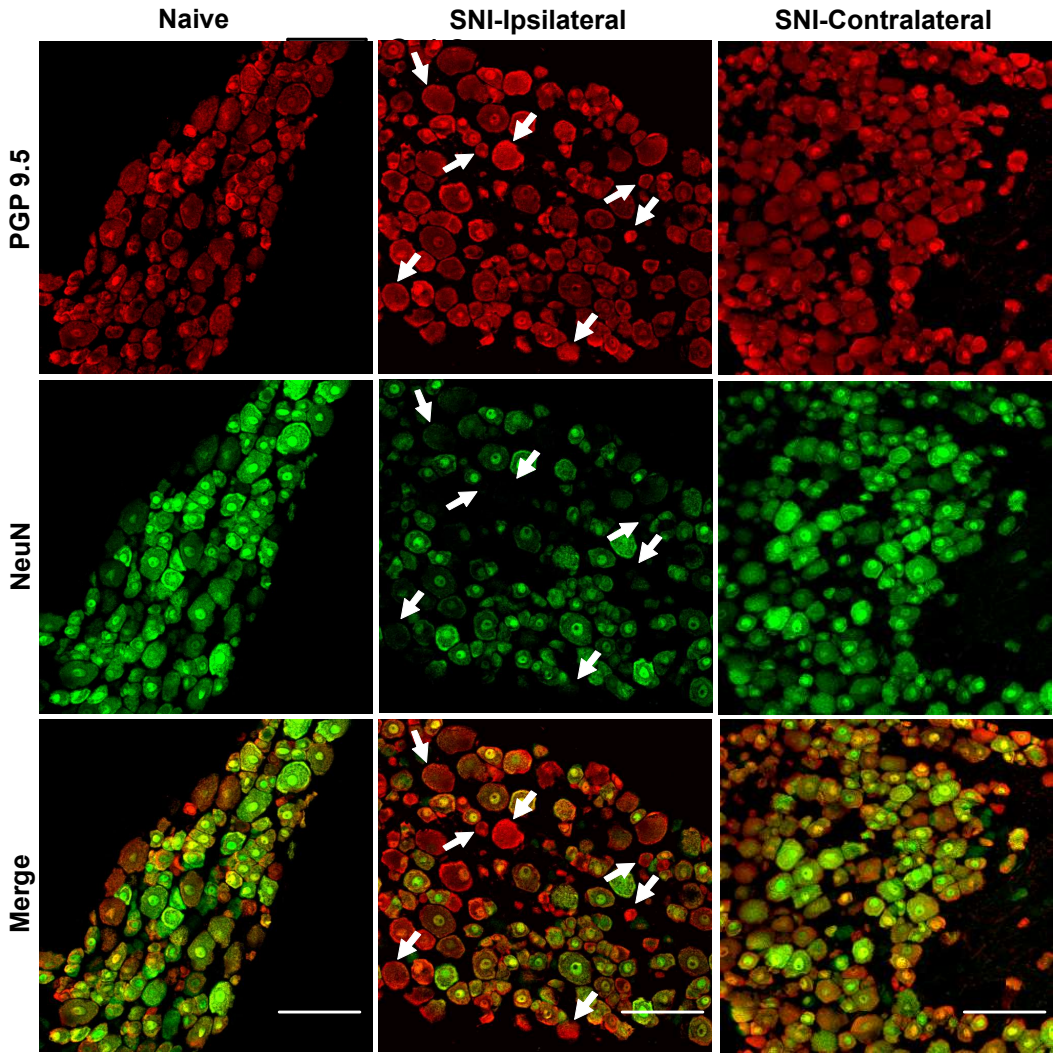

Suppl. Fig. 4. The staining of the neuronal marker PGP 9.5 is stable after spared nerve injury (SNI), whereas NeuN expression was reduced or absent in some DRG neurons ipsilateral to the injury. Representative microphotographs from double immunostaining for PGP 9.5 (red) and NeuN (green) in L4 DRG from naive mice, and ipsilateral and contralateral L4 DRG from mice with SNI 7 days after surgery. Arrows indicate neurons with decreased NeuN staining and clear PGP 9.5 labeling. Scale bar 100 µm.